# NACA

# RESEARCH MEMORANDUM

THE EFFECTIVE DOWNWASH CHARACTERISTICS AT TRANSONIC

SPEEDS OF A 6-PERCENT-THICK WING WITH 47° OF SWEEPBACK
IN COMBINATION WITH A CYLINDRICAL BODY AS DETERMINED FROM

FORCE MEASUREMENTS OF A HORIZONTAL TAIL

By Domenic A. Coppolino

Langley Aeronautical Laboratory Langley Field, Va.

CLASSIFIED DOCUMENT

This material contains information affecting the National Defense of the United States within the meani of the espionage laws, Title 18, U.S.C., Secs. 793 and 794, the transmission or revelation of which in a manner to unauthorized person is prohibited by law.

# NATIONAL ADVISORY COMMITTE

WASHINGTON

November 26, 1952

### NATIONAL ADVISORY COMMITTEE FOR AERONAUTICS

#### RESEARCH MEMORANDUM

THE EFFECTIVE DOWNWASH CHARACTERISTICS AT TRANSONIC

SPEEDS OF A 6-PERCENT-THICK WING WITH 47° OF SWEEPBACK

IN COMBINATION WITH A CYLINDRICAL BODY AS DETERMINED FROM

FORCE MEASUREMENTS OF A HORIZONTAL TAIL

By Domenic A. Coppolino

#### SUMMARY

The effective downwash characteristics of a wing-body configuration and the body alone were determined from lift measurements of a horizontal tail located 0.333 and 0.479 wing semispan above the body center line. The wing had a sweepback angle of 47°, an aspect ratio of 3.5, a taper ratio of 0.2, and a thickness ratio of 0.06. The plan form of the horizontal tail was geometrically similar to that of the wing. The investigation was made in the Langley 8-foot transonic tunnel.

At low angles of attack (-2° to 5°), the rate of change of effective downwash angle with angle of attack was approximately 0.1 less for the horizontal tail located 0.479 wing semispan above the body center line than for the horizontal tail located 0.333 wing semispan above the body center line. The rate of change of effective downwash angle with angle of attack for the wing-body configuration at high angles of attack (9° to 12°) was approximately twice that at low angles of attack (-2° to 5°) and exceeded 1.0 at subsonic Mach numbers greater than 0.65.

#### INTRODUCTION

A knowledge of the effective downwash characteristics in the region of the horizontal tail is necessary in order to determine the contribution of the downwash to the longitudinal stability of airplanes at transonic speeds. Some effects of wing plan form and thickness on the transonic downwash characteristics for wing and wing-fuselage configurations are reported in reference 1. Reference 2 reports an investigation at transonic speeds of the force and moment characteristics of several wings in combination with a cylindrical body of ogival nose section. The body

shape used in that investigation was selected mainly on considerations of simplicity rather than in an attempt to approximate a specific fuse-lage design. During the tests of one of the wings and of the body alone, a horizontal tail was mounted on the sting behind the body and, in addition to the measurements of the forces and moments of the wing-body configuration, the lift of the horizontal tail was measured on a two-component strain-gage balance. The horizontal-tail lift measurements were used in determining effective downwash angles and form the basis of the present paper.

Presented herein are effective downwash angles for the wing-body configuration and the body alone at Mach numbers from 0.50 to approximately 1.11. The wing had a sweepback angle of 47° based on the 0.25-chord line, an aspect ratio of 3.5, a taper ratio of 0.2, and an NACA 65A006 thickness distribution cambered for a design lift coefficient of 0.1. The horizontal tail had a plan form similar to that of the wing but had an NACA 65A009 airfoil section at the root and an NACA 65A005 airfoil section at the tip. Two positions of the horizontal tail above the body center line were investigated. The scope of the downwash investigation was largely governed by the scope of the wing investigation, and this limitation resulted in abbreviated downwash studies. The data although incomplete are believed to warrant publication since they add to the information on downwash at transonic speeds.

#### SYMBOLS

0.1	$N_t \cos(\alpha' + i)$
CLt	lift coefficient of horizontal tail, $\frac{N_t \cos(\alpha' + i)}{qS_t}$
dC <sub>Lt</sub>	lift-curve slope of horizontal tail
di	
Ъ	span of wing
bt	span of horizontal tail
С	section chord of wing
ct	section chord of horizontal tail
₹	mean aerodynamic chord of wing based on relationship, $\frac{2}{5}\int_0^{b/2}c^2\mathrm{d}y$

ē t	mean aerodynamic chord of horizontal tail based on relationship, $\frac{2}{S_t} \int_0^{b_t/2} c_t^2 dy$
ht	height of horizontal tail above body center line
Nt	normal force of horizontal tail
M	free-stream Mach number
g	free-stream dynamic pressure, $\frac{1}{2}\rho V^2$
R	Reynolds number based on mean aerodynamic chord
S	area of wing
St	area of horizontal tail
V	free-stream velocity
У	spanwise distance from plane of symmetry
α	angle of attack of body, based on center line of body
α'	angle of attack of sting support, measured by angle between center line of sting support and direction of undisturbed stream
i	angle of horizontal tail with respect to center line of sting support
E	effective downwash angle
ρ	free-stream density

### APPARATUS AND MODELS

### Tunnel

The tests were conducted in the slotted test section of the Langley 8-foot transonic tunnel. The use of longitudinal slots in the test section permits the testing of a model through the speed of sound without the usual choking effects found in the conventional closed-throat type

of wind tunnel. Typical Mach number distributions along the center line of the slotted test section in the region occupied by the model and taken from reference 3 are shown in figure 1. A more complete description of the slotted test section of the Langley 8-foot transonic tunnel may be found in reference 3.

#### Models

The models employed for the tests were constructed of steel and were supplied by a U. S. Air Force contractor. The horizontal tail had an NACA 65A009 airfoil section at the root and an NACA 65A005 airfoil section at the tip parallel to the plane of symmetry, 47° of sweepback of the 0.25-chord line, an aspect ratio of 3.5, and a taper ratio of 0.2. The wing had a plan form geometrically similar to that of the horizontal tail, had a thickness ratio of 6 percent parallel to the model plane of symmetry, and had the following airfoil section parallel to the model plane of symmetry:

Thickness distribution - NACA 65A006

Mean line ordinates - 1/3 of NACA 230 series plus NACA 6-series uniform-load mean line (a = 1.0) for a design lift coefficient of 0.1

The fuselage was a cylindrical body with an ogival nose section, and the ratio of body diameter to wing span was 0.094. A photograph of the model is shown as figure 2 and dimensional details are shown in figure 3.

The horizontal tail was tested in two positions above the center line of the body. One position of the horizontal tail was located 0.333 wing semispan above the body center line and the other position was 0.479 wing semispan above the body center line, with the quarterchord point of the mean aerodynamic chord of the horizontal tail located 1.217 wing semispans rearward of the quarter-chord point of the mean aerodynamic chord of the wing for both positions. The horizontal tail was attached to a two-component electrical strain-gage balance which was housed in a cylindrical boom, the center line of which was parallel to the center line of the sting support. The boom was fastened to the sting support with a 45° sweptforward symmetrical steel strut of 0.0833 thickness ratio. The incidence of the horizontal tail was varied by rotating the tail and cylindrical boom about an axis which passed through the quarter-chord point of the mean aerodynamic chord of the tail. The wingbody configuration was attached to the sting support through a sixcomponent internal electrical strain-gage balance.

The angle of attack of the body was varied by pivoting the sting support (fig. 3) about an axis approximately 66 inches downstream of the

25-percent point of the mean aerodynamic chord of the wing. In order to keep the model position reasonably close to the tunnel axis when the model angle of attack was varied from 6° to 12°, a 15° coupling was inserted upstream of the pivot point. The angle-of-attack mechanism was remotely controlled which permitted angle-of-attack changes with the tunnel operating. A more detailed description of the support system is given in reference 4.

A pendulum-type accelerometer, calibrated against angle of attack  $\alpha'$  of the sting support and located within the sting support downstream of the model permitted the angle of attack of the sting support to be set within  $\pm 0.1^{\circ}$  at all test Mach numbers.

#### TESTS

The Reynolds numbers based on the mean aerodynamic chords of the horizontal tail and wing and averaged for several runs is shown in figure 4 as a function of test Mach number. The Reynolds number for the horizontal tail varied from 663,000 at a Mach number of 0.50 to 851,000 at a Mach number of 1.10. The Reynolds number for the wing varied from  $2.0 \times 10^6$  to  $2.5 \times 10^6$  for the same range of Mach numbers.

#### Measurements

The lift of the horizontal tail was obtained simultaneously with the six-component data for the wing-body configuration. The aerodynamic characteristics for the wing-body configuration can be found in reference 2. The range of variables for the horizontal-tail investigation was dependent on the test conditions for the wing-body configuration and, as a result, a complete investigation of the horizontal tail was not obtained. The following table summarizes the range of data obtained:

Configuration	Tail height, h <sub>t</sub>	Tail incidence (deg)	a' range (deg)	M range
Wing-body Wing-body Wing-body Wing-body Wing-body Body alone Body alone	0.333b/2 0.333b/2 0.333b/2 0.333b/2 0.479b/2 0.479b/2	0 0 -3, 3 -3 0 0	-2 to 12 -2 to 4 4 to 12 4 -2 to 4 -2 to 12 -2 to 12	1.024 to 1.112

## Corrections and Accuracy

No corrections to the free-stream Mach number and dynamic pressure for the effects of model and wake blockage are necessary for tests in the slotted test section of the 8-foot transonic tunnel (ref. 5). There is a range of Mach numbers above a Mach number of 1.00, however, where the data are affected by the reflected compressions and expansions from the test-section boundary. Based on the results of reference 6, it is believed that for Mach numbers up to approximately 1.04 the effects of these disturbances on the measurements made in the present investigation may be considered to be negligible. For test Mach numbers above 1.04, however, the data were influenced by the boundary-reflected disturbances, but the extent to which the data were affected by the reflected disturbances is not known for these tests. At a Mach number of 1.088 and above, the boundary-reflected disturbances struck the horizontal tail as shown by schlieren photographs (not presented herein) taken during the tests. The validity of the data above a Mach number of 1.04, therefore, should be considered to be impaired.

The reference axes of the data presented in the figures have been changed from body axes to wind axes. Since the horizontal tail was instrumented with only a two-component electrical strain-gage balance which measured the normal force but not the axial force, the conversion from body axes to wind axes was computed by neglecting the small contribution to the lift component of the axial force.

The accuracy of the balance based on the design of the horizontal-balance and the repeatability of the data is  $\pm 0.005$  for  $\text{C}_{\text{L}_{\text{t}}}$ .

#### DOWNWASH CALCULATIONS

The effective downwash angle was determined from the relation:

$$\alpha_t = \alpha^t + i - \epsilon$$

where  $\alpha_t$  is the local angle of attack of the horizontal tail. When  $CL_t=0$ , it is assumed that  $\alpha_t=0^{\circ}$  and, therefore,

$$\epsilon = \alpha' + (i)_{C_{L_{+}}=0}$$
 (1)

or

$$\epsilon = i + (\alpha^{\dagger})_{C_{L_{t}}=0}$$
CONFIDENTIAL

In determining the effective downwash angle the assumption was made that the ratio of the dynamic pressure at the horizontal tail to the free-stream dynamic pressure was 1.00. Since a horizontal-tail incidence of only 0° was tested for the horizontal tail in both positions in the presence of the body alone and for the horizontal tail located 0.479 wing semispan above the body center line in the presence of the wing-body con-

figuration, the lift-curve slope  $\frac{dC_{L_t}}{di}$  was not determined for these con-

figurations. In obtaining the effective downwash angle for these configu-

rations, it was assumed that the lift-curve slope  $\frac{dC_{L_t}}{di}$  was the same as

that obtained for the horizontal tail located 0.333 wing semispan above the body center line in the presence of the wing-body configuration. Also, since it is possible that a loss in tail lift-curve slope occurs at high angles of attack the evaluation of the effective downwash angle at high angles of attack can be misleading. It is believed, however, that the values of the effective downwash angle presented for the wing-body configuration at high angles of attack may be valid because the effective downwash angle is large and the local tail angle may be relatively small, but in the case of the body alone, the data at high angles may be invalid and therefore are not presented. It should be realized that the effective downwash angle presented herein is modified by the mutual interference effects of the boom, the horizontal tail, the vertical strut, and the sting support.

# PRESENTATION OF RESULTS AND DISCUSSION

In order to facilitate presentation of the data, staggered scales have been used in many of the figures and care should be taken in identifying the zero axis for each curve.

The variation with angle of attack  $\alpha'$  of the horizontal-tail lift coefficient for the two tail positions in the presence of the wing-body and body alone configurations is presented in figures 5 to 10. Figures 11 to 16 show the variation for the wing-body and body alone configurations of angle of attack  $\alpha'$  with body angle of attack caused by the flexibility of the sting-support system. The variation with Mach number of

the lift-curve slope  $\frac{dC_{L_t}}{di}$  (averaged over the incidence range) at an angle of attack  $\alpha'$  of  $4^{\circ}$  is given in figure 17. The values of the tail lift-curve slope shown in figure 17 were used to determine the effective downwash angles and these results for both tail heights are presented in figures 18 and 19 for the wing-body and body alone configurations, respectively.

8

The effect of Mach number on the rate of change of downwash angle with angle of attack for the wing-body and body alone configurations is presented in figure 20 for the two positions of the horizontal tail. The effective downwash derivative  $\frac{\partial \epsilon}{\partial \alpha}$  for the body alone was essentially

the same for both positions of the horizontal tail at the low angles of attack  $(-2^{\circ})$  to approximately  $5^{\circ}$ ) throughout the Mach number range. The value of the downwash derivative was small and decreased approximately 0.15 through the transonic speed range.

At low body angles of attack (-2° to 5°) the downwash derivative for the wing-body configuration for both positions of the horizontal tail showed a gradual increase as the speed was increased up to a Mach number of 0.93, followed by a rapid decrease through the transonic speed range (fig. 20). This decrease was due in part to the loss of lift-curve slope of the wing-body configuration as indicated in reference 2 and in part to the decrease of the downwash derivative for the body alone as discussed previously. Figure 20 shows that the downwash derivative  $\frac{\partial \epsilon}{\partial \alpha}$  for the horizontal tail located 0.479 wing semispan above the body center line was approximately 0.1 less than that for the horizontal tail located 0.333 wing semispan above the body center line throughout the Mach number range which is in agreement with theory and indicated experimentally in reference 4. The results at a Mach number of 0.50 were compared with theory (ref. 7) and the agreement was good. The spanwise lift distributions necessary for these calculations were obtained using reference 8.

Figure 20 also shows that in the high angle-of-attack range (9° to 12°) the wing-body downwash derivative was approximately twice that for the low angle-of-attack range. It is to be noted that at subsonic speeds above a Mach number of 0.65, the derivative  $\frac{\partial \epsilon}{\partial \alpha}$  was greater than 1.0. For the complete airplane, the increase in the derivative  $\frac{\partial \epsilon}{\partial \alpha}$  would indicate a destabilizing effect which would aggravate the unstable characteristics of the wing-body configuration at lift coefficient near 0.6 as reported in reference 2.

#### CONCLUSIONS

An investigation was made in the Langley 8-foot transonic tunnel of a horizontal tail in the presence of a wing-body configuration and the body alone. The horizontal tail was tested in two positions above the body center line. The wing had a sweepback angle of 47°, an aspect ratio of 3.5, a taper ratio of 0.2, and a thickness ratio of 0.06. The

horizontal tail had a plan form geometrically similar to that of the wing. The body was cylindrical with an ogival nose. The following conclusions were noted:

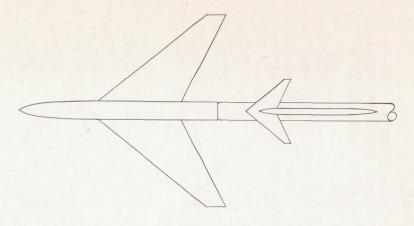
- 1. The rate of change of effective downwash angle with angle of attack for the wing-body configuration at low angles of attack (-2° to 5°) was approximately 0.1 less for the horizontal tail located 0.479 wing semispan above the body center line than for the horizontal tail located 0.333 wing semispan above the body center line. For the body alone, the downwash derivative was essentially the same for both positions of the horizontal tail at the low angles of attack.
- 2. The rate of change of effective downwash angle with angle of attack for the wing-body configuration in the high angle-of-attack range (9° to 12°) was approximately twice that at low angles of attack (-2° to 5°) and exceeded 1.0 at subsonic Mach numbers greater than 0.65.

Langley Aeronautical Laboratory,
National Advisory Committee for Aeronautics,
Langley Field, Va.

#### REFERENCES

- 1. Weil, Joseph, Campbell, George S., and Diederich, Margaret S.: An Analysis of Estimated and Experimental Transonic Downwash Characteristics as Affected by Plan Form and Thickness for Wing and Wing-Fuselage Configurations. NACA RM L52I22, 1952.
- 2. Bielat, Ralph P., Harrison, Daniel E., and Coppolino, Domenic A.: An Investigation at Transonic Speeds of the Effects of Thickness Ratio and of Thickneed Root Sections on the Aerodynamic Characteristics of Wings With 47° Sweepback, Aspect Ratio 3.5, and Taper Ratio 0.2 in the Slotted Test Section of the Langley 8-Foot High-Speed Tunnel. NACA RM L51104a, 1951.
- 3. Wright, Ray H., and Ritchie, Virgil S.: Characteristics of a Transonic Test Section With Various Slot Shapes in the Langley 8-Foot High-Speed Tunnel. NACA RM L51H10, 1951.
- 4. Osborne, Robert S.: A Transonic-Wing Investigation in the Langley 8-Foot High-Speed Tunnel at High Subsonic Mach Numbers and at a Mach Number of 1.2. Wing-Fuselage Configuration Having a Wing of 45° Sweepback, Aspect Ratio 4, Taper Ratio 0.6, and NACA 65A006 Airfoil Section. NACA RM L50H08, 1950.
- 5. Wright, Ray H., and Ward, Vernon G.: NACA Transonic Wind-Tunnel Test Sections. NACA RM L8J06, 1948.
- 6. Ritchie, Virgil S., and Pearson, Albin O.: Calibration of the Slotted Test Section of the Langley 8-Foot Transonic Tunnel and Preliminary Experimental Investigation of Boundary-Reflected Disturbances.

  NACA RM L51K14, 1952.
- 7. Diederich, Franklin W.: Charts and Tables for Use in Calculations of Downwash of Wings of Arbitrary Plan Form. NACA TN 2353, 1951.
- 8. DeYoung, John: Theoretical Additional Span Loading Characteristics of Wings With Arbitrary Sweep, Aspect Ratio, and Taper Ratio. NACA TN 1491, 1947.



Diffuser-entrance-nose arrangement for subsonic operation
Diffuser-entrance-nose arrangement for supersonic operation

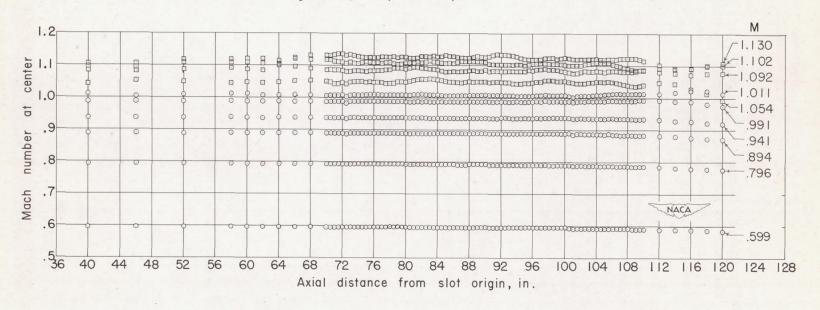


Figure 1.- Mach number distributions along the center of the test section.

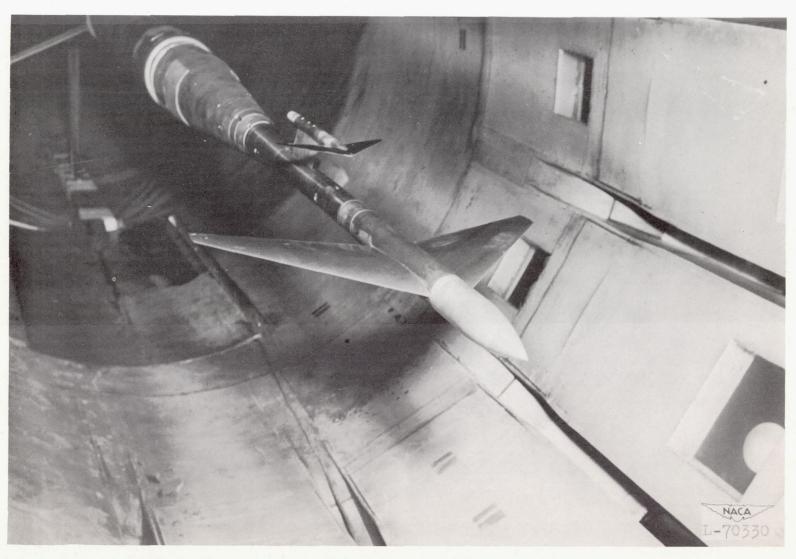
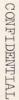


Figure 2.- Model as tested in the Langley 8-foot transonic tunnel.



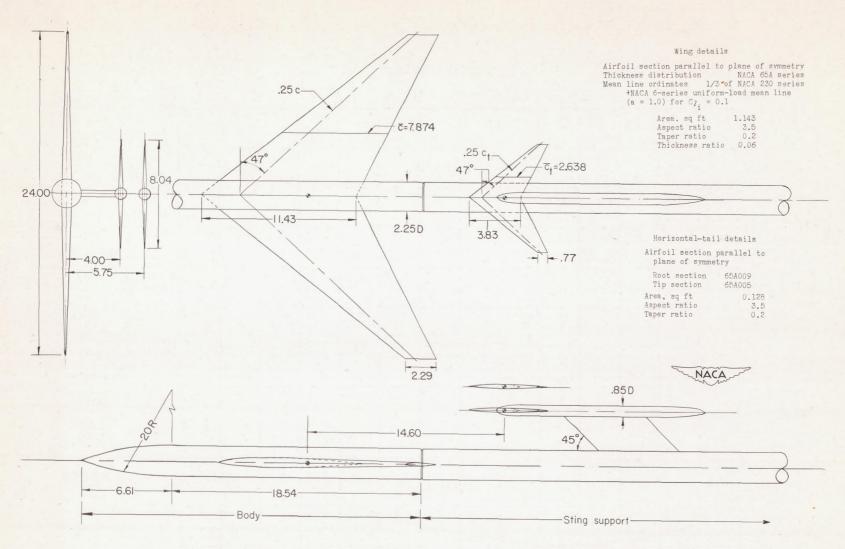


Figure 3.- Model details. All dimensions are in inches.

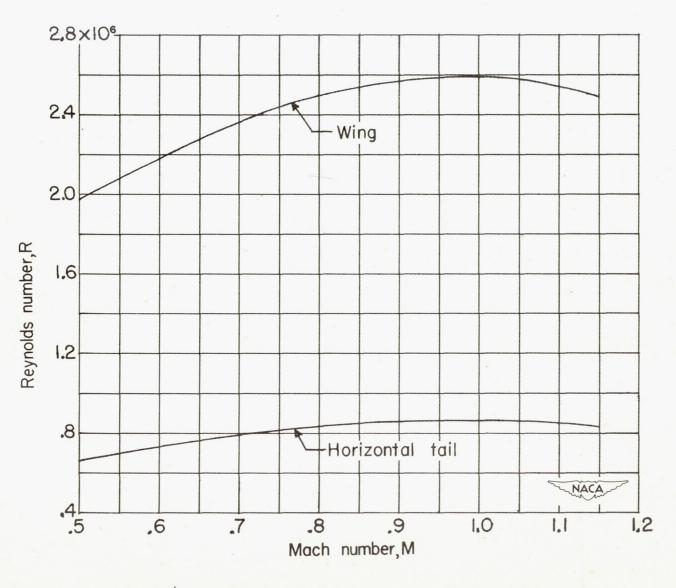


Figure 4.- Variation with Mach number of test Reynolds number.

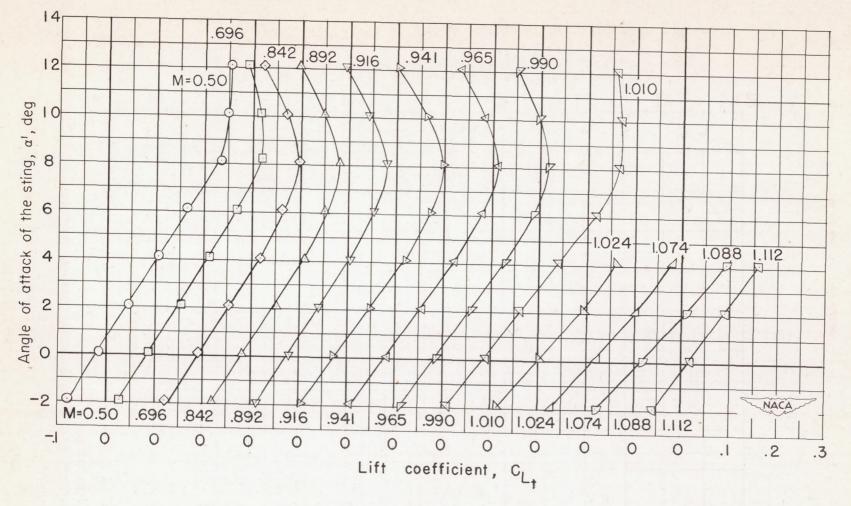


Figure 5.- Variation of the angle of attack of the sting with the horizontal-tail lift coefficient in presence of the wing-body configuration.  $h_t = 0.333\frac{b}{2}$ ;  $i = 0^{\circ}$ .

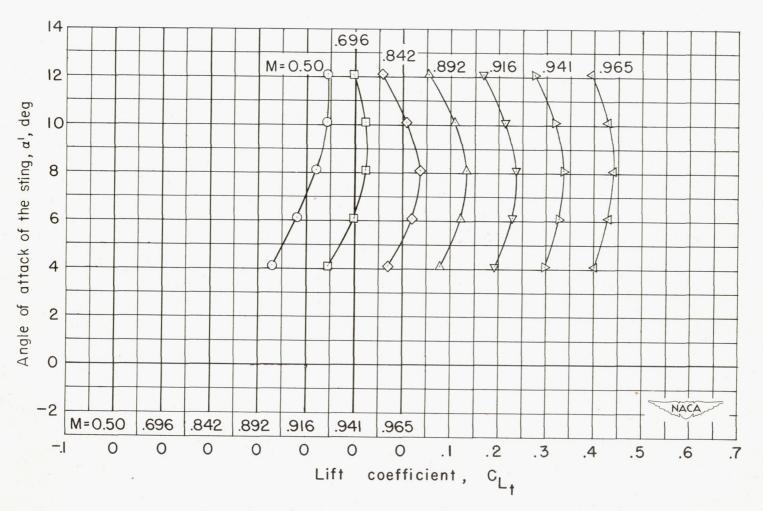


Figure 6.- Variation of the angle of attack of the sting with the horizontal-tail lift coefficient in presence of the wing-body configuration.  $h_t = 0.333\frac{b}{2}$ ;  $i = 3^{\circ}$ .

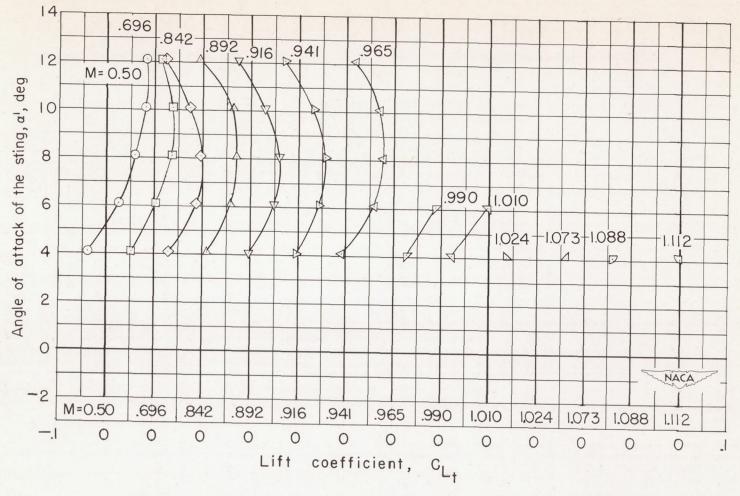


Figure 7.- Variation of the angle of attack of the sting with the horizontal-tail lift coefficient in presence of the wing-body configuration.  $h_t = 0.333\frac{b}{2}$ ;  $i = -3^{\circ}$ .

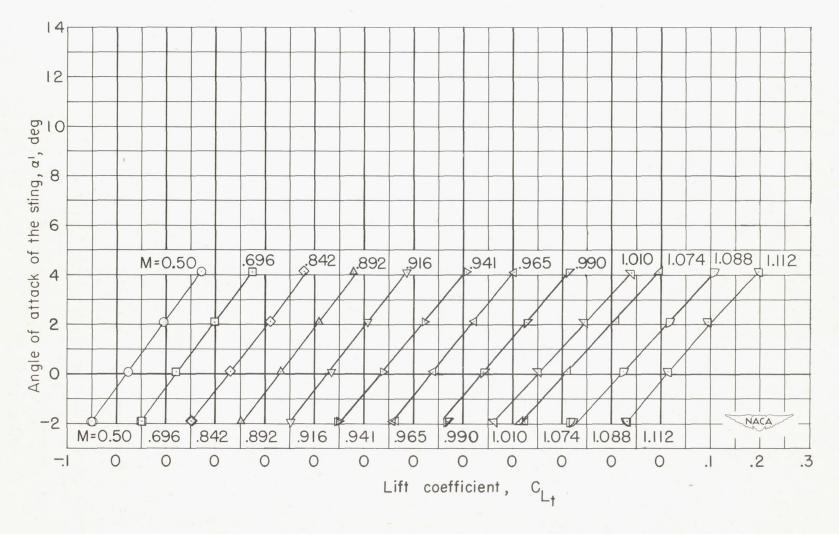


Figure 8.- Variation of the angle of attack of the sting with the horizontal-tail lift coefficient in presence of the wing-body configuration.  $h_t = 0.479\frac{b}{2}$ ;  $i = 0^{\circ}$ .

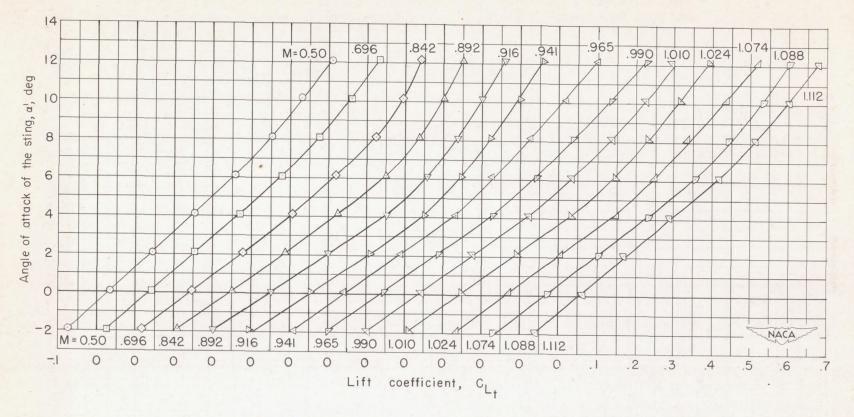


Figure 9.- Variation of the angle of attack of the sting with the horizontal-tail lift coefficient in presence of the body alone.  $h_t = 0.333\frac{b}{2}$ ;  $i = 0^{\circ}$ .

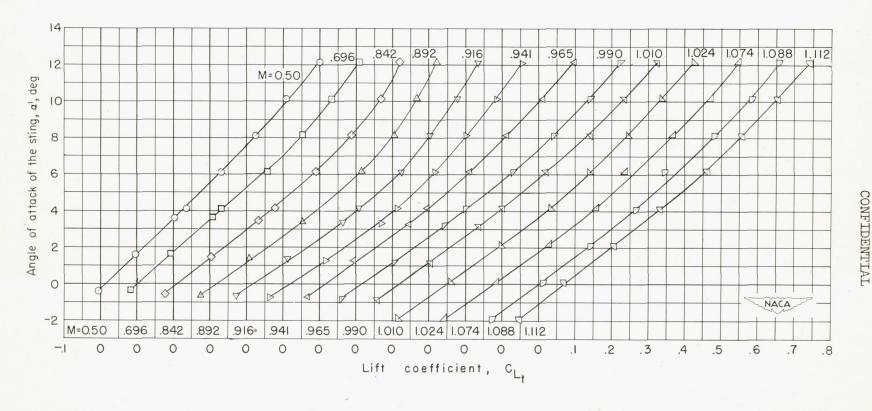


Figure 10.- Variation of the angle of attack of the sting with the horizontal-tail lift coefficient in presence of the body alone.  $h_t = 0.479\frac{b}{2}$ ;  $i = 0^{\circ}$ .

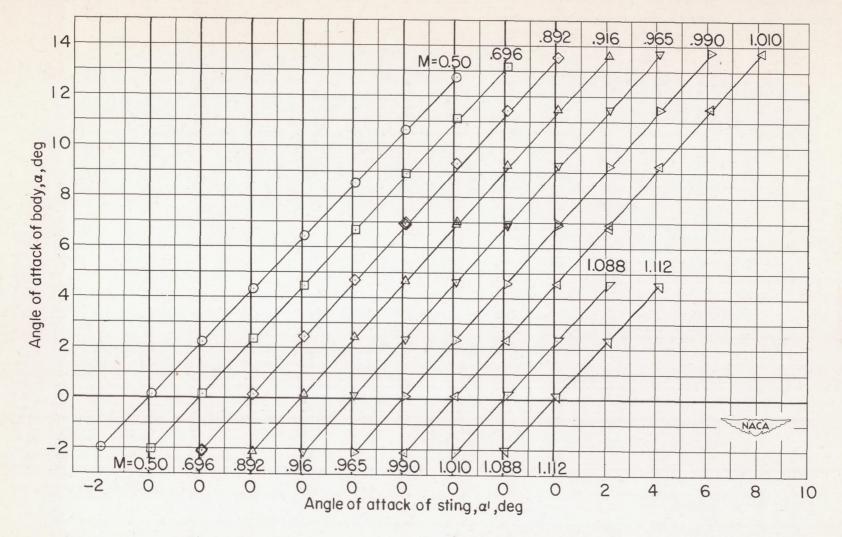


Figure 11.- Variation of angle of attack of body with angle of attack of sting. Wing-body configuration;  $h_t = 0.333\frac{b}{2}$ ;  $i = 0^{\circ}$ .

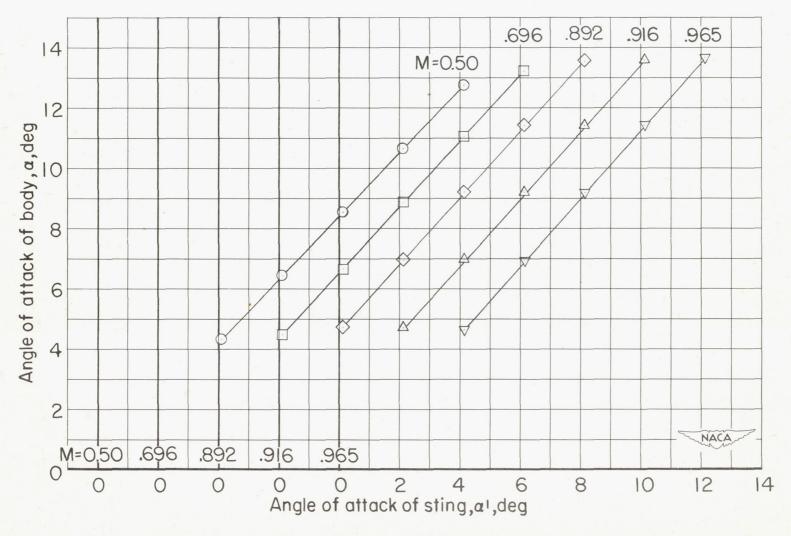


Figure 12.- Variation of angle of attack of body with angle of attack of sting. Wing-body configuration;  $h_t = 0.333\frac{b}{2}$ ;  $i = 3^{\circ}$ .

NACA RM L52J15

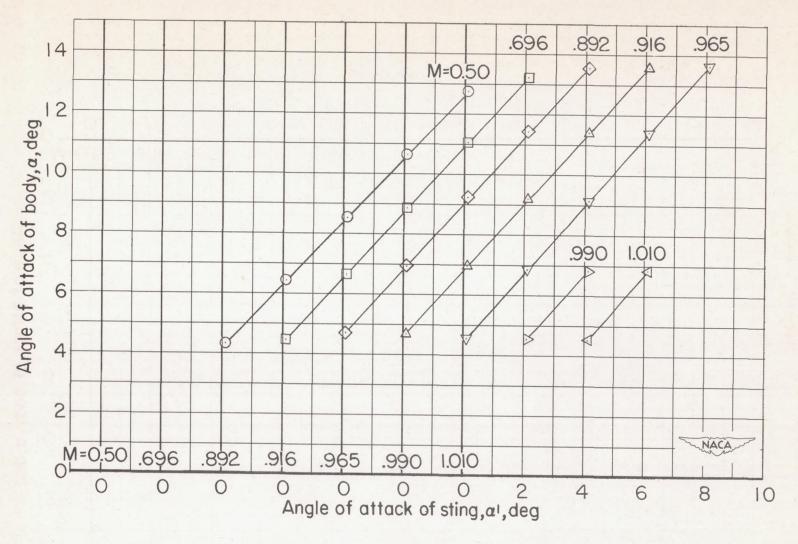


Figure 13.- Variation of angle of attack of body with angle of attack of sting. Wing-body configuration;  $h_t = 0.333\frac{b}{2}$ ;  $i = -3^{\circ}$ .

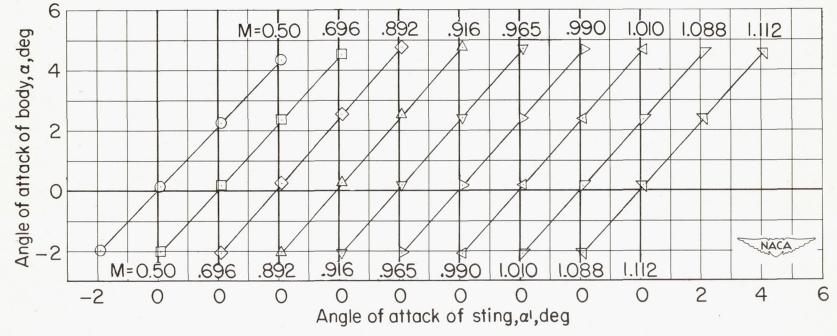


Figure 14.- Variation of angle of attack of body with angle of attack of sting. Wing-body configuration;  $h_t = 0.479\frac{b}{2}$ ;  $i = 0^{\circ}$ .

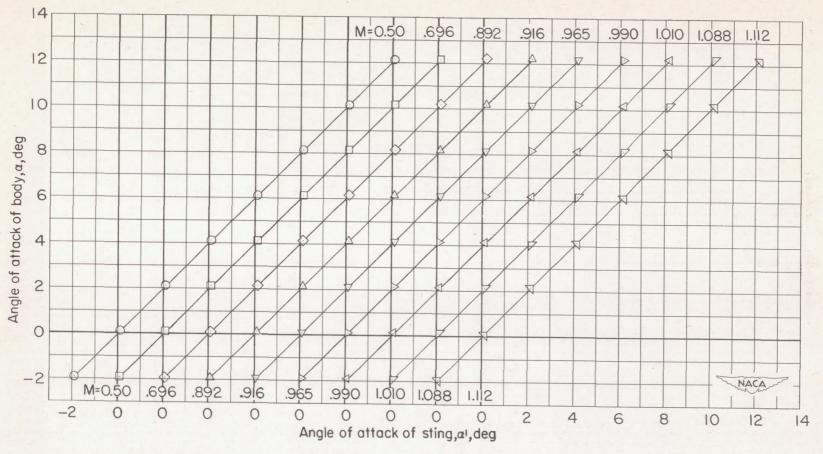


Figure 15.- Variation of angle of attack of body with angle of attack of sting. Body alone;  $h_t = 0.333\frac{b}{2}$ ;  $i = 0^{\circ}$ .

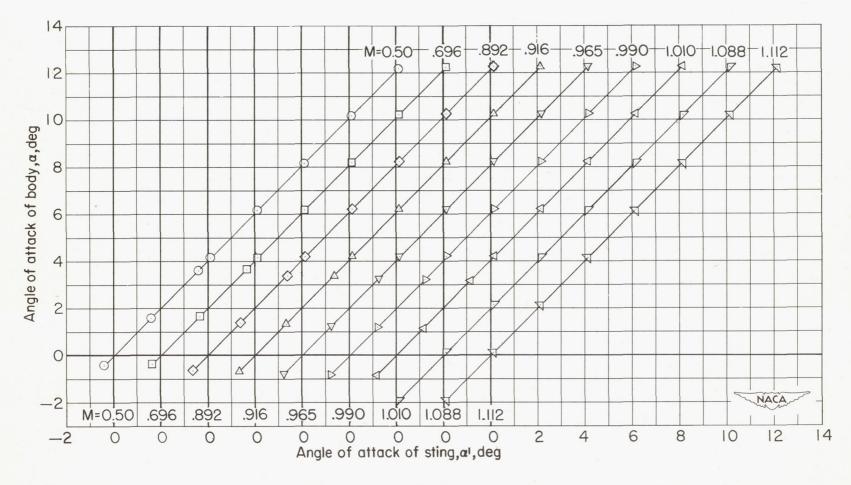


Figure 16.- Variation of angle of attack of body with angle of attack of sting. Body alone;  $h_t = 0.479\frac{b}{2}$ ;  $i = 0^{\circ}$ .

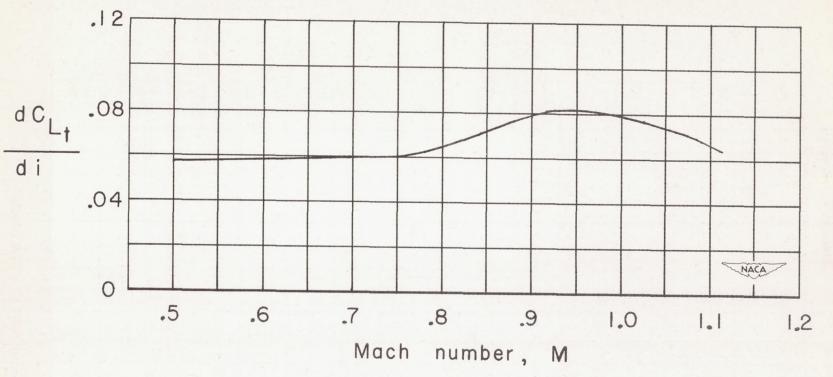


Figure 17.- Variation of the horizontal-tail lift-curve slope with Mach number in presence of the wing-body configuration.  $\alpha' = \mu^{\circ}$ .

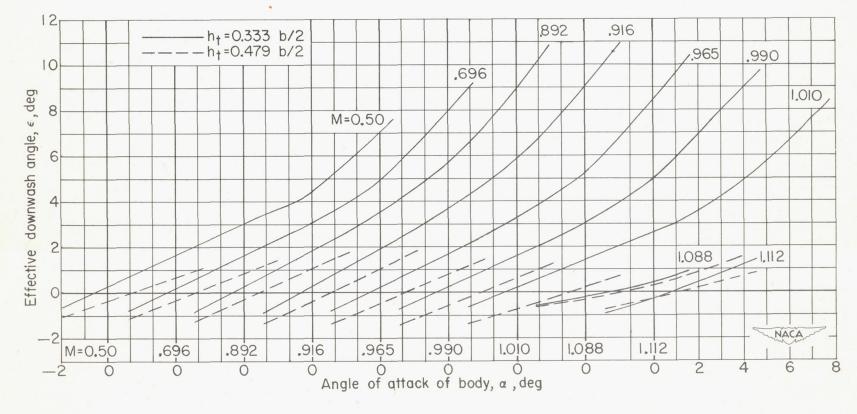


Figure 18. - Variation with angle of attack of body of the effective downwash angle for the wing-body configuration.

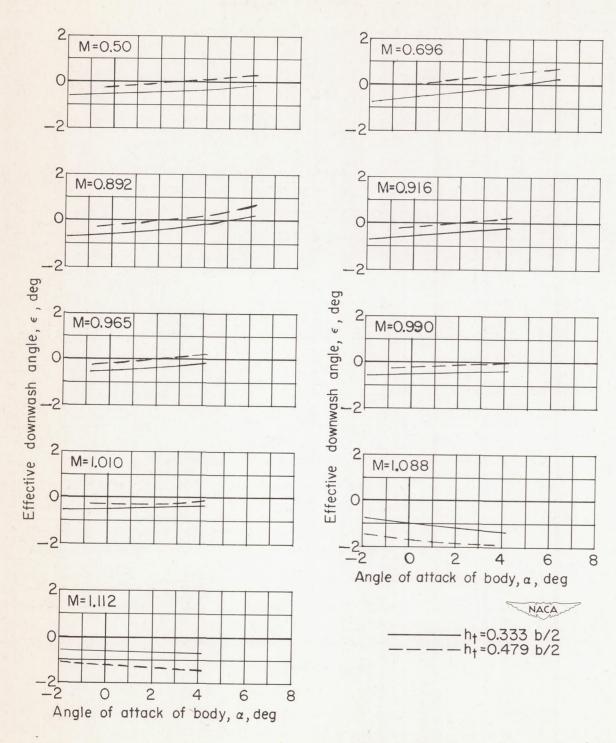


Figure 19.- Variation with angle of attack of body of the effective downwash angle for the body alone.

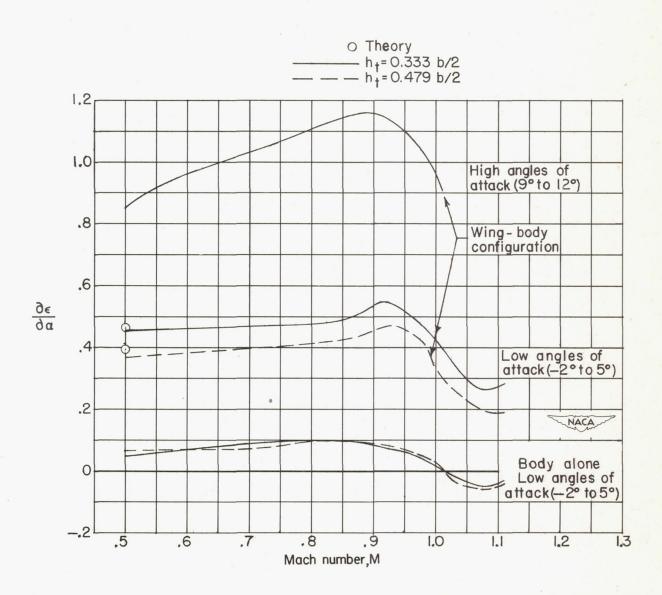


Figure 20. - Variation with Mach number of the effective downwash derivative for the wing-body and body alone configurations.

# SECURITY INFORMATION CONFIDENTIAL